Soft Matter

Diffusive ferromagnetic roller gas

Journal:	*Soft Matter*
Manuscript ID	SM-ART-02-2019-000274.R1
Article Type:	Paper
Date Submitted by the Author:	27-Mar-2019
Complete List of Authors:	Kokot, Gasper; Argonne National Laboratory, Materials Science Division Vilfan, Andrej; Jozef Stefan Institute Glatz, Andreas; Argonne National Laboratory, Materials Science Division Snezhko, Alexey; Argonne National Laboratory

ROYAL SOCIETY OF CHEMISTRY

ARTICLE TYPE

Cite this: DOI: 10.1039/xxxxxxxxxx

Diffusive ferromagnetic roller gas†

Gašper Kokot,[a] Andrej Vilfan,[b,c] Andreas Glatz,[a,d] and Alexey Snezhko*[a]

Received Date
Accepted Date

DOI: 10.1039/xxxxxxxxxx

www.rsc.org/journalname

An ensemble of actively rotating ferromagnetic particles is used to realize an active roller gas. Here, we investigate the diffusive properties of such a gas in experiments and simulations. We reveal that ferromagnetic rollers demonstrate a normal (Fickian) diffusion with a characteristic linear growth of the mean-squared displacement, while statistics of displacements stay non-Gaussian. At short times the system has a bimodal distribution of the displacements that transitions with time to a quasi-Gaussian distribution (Gaussian core with overpopulated tails) for a range of studied particle number densities. Inert particles introduced into the active roller gas exhibit similar diffusive behavior. The results provide insights into diffusive properties of active colloidal systems with activity originating from spinning degrees of freedom.

1 Introduction

Active colloids use energy from the environment to maintain out-of-equilibrium states [1–6]. Recently it has been demonstrated [7–9] that statistical properties of active colloidal/granular systems, specifically diffusion, may significantly deviate from classical Brownian processes. In a number of reported out-of-equilibrium systems it has been observed that "normal" – linear in time – behavior of the mean-squared displacement (MSD) was often accompanied by a non-Gaussian displacement distribution [7,10–13]. The behavior was attributed to the distribution of diffusivities of individual particles in the ensemble [7,14,15].

Up to this point most of the related experimental studies have been performed in realizations of active colloids based only on the translational motion of individual units while systems with activities originating from spinning remained unexplored. Recent advances in the design of active colloidal systems based on spinning enable an experimental access to large systems with activities stemming from the rotation of particles [5,16–18]. In the present paper, we investigate the displacement statistics of particles in a quasi-two-dimensional active roller gas, realized by means of ferromagnetic particles spontaneously rolling in a uniaxial alternating magnetic field in a certain range of excitation frequencies [17,19]. We compare experimental observations to the predictions of discrete particle simulations. We show that at short times the system has a bimodal distribution of the displacements that transitions with time into a quasi-Gaussian distribution (Gaussian core with overpopulated tails) for all studied particle number densities. The non-Gaussian nature of the displacement statistics is also captured by the time evolution of the distribution kurtosis. We reveal that the non-Gaussian displacement statistics of the ferromagnetic roller gas is accompanied by a normal (Fickian) diffusion with linear growth of the mean-squared displacement. Our experimental observations are confirmed by simulations.

2 Experimental methods and model

2.1 Magnetic roller gas

In our experiments we use ferromagnetic nickel spheres (with $125-150\,\mu$m uniform diameter distribution) sedimented at the bottom of a flat bottom glass container (5 cm diameter) filled with deionised water with 0.1% v/v Tween 80 solution added to charge stabilize the particles. A uniform vertical alternating magnetic field ($B_z = B_0 \sin(\omega_0 t)$, where $B_0 = 5.8\,$mT is the amplitude and $\omega_0 = 2\pi f_0 = 2\pi \cdot 60\,\mathrm{s}^{-1}$ is the angular frequency) is applied to energise the ensemble. The magnetic moment per particle is $\mu \approx 0.02\,\mu\mathrm{A\,m}^2$. The rolling motion of particles emerges as a spontaneous symmetry breaking of the clockwise/counterclockwise rotations experienced by a magnetic sphere in a uniaxial alternating field in a certain range of excitation parameters [17,20]. There are two primary mechanisms that may lead to a steady rolling motion of the particles. When the field direction changes, the particles rotate. Because of the inertia, the rotation overshoots and during the next field oscillation the rotation tend to continue around the same axis. Spherical particles steadily spin when the following condition is satisfied: $\mathrm{Im}\left(\nu\left[-p^2, 2q\right]\right) - p > 0$ [17]. Here the characteristic Mathieu exponent ν is a function of the two parameters $p = \alpha_r/(\omega I)$ and $q = \mu B_0/(\omega^2 I)$, where $\omega = 2\pi f_B$, η

[a] Materials Science Division, Argonne National Laboratory, 9700 S Cass Avenue, Lemont, IL 60439, USA
[b] Max Planck Institute for Dynamics and Self-Organization, Göttingen, Germany
[c] J. Stefan Institute, Jamova 39, 1000 Ljubljana, Slovenia
[d] Department of Physics, Northern Illinois University, DeKalb, IL 60115, USA
* Corresponding author. E-mail: snezhko@anl.gov

† Electronic Supplementary Information (ESI) available: [details of any supplementary information available should be included here]. See DOI: 10.1039/b000000x/

is the fluid's dynamic viscosity and μ, m, $I=\frac{2}{5}mR_{\rm Ni}^2$, $\alpha_{\rm r}=8\pi\eta R_{\rm Ni}^3$ are correspondingly the magnetic moment, mass, moment of inertia, and the rotational drag coefficient of a roller. In the state of a steady rotation, the magnetic torque on the particle, $T_{\rm m}=\|\boldsymbol{\mu}\times\mathbf{B}\|$, is balanced by its viscous torque, $T_{\rm v}\simeq\alpha_{\rm r}\omega$. A similar, more robust steady rotation can also result from a particle shape anisotropy, if such anisotropic particle sediment with an orientation that is not aligned with the magnetization (see Model and Simulation). The frequency of the alternating magnetic field controls the speed of the rolling motion and is used to tune the activity of the system. Because the magnetic field in our experiments oscillates perpendicularly to the surface (see Fig. 1a), the direction of rolling is randomly chosen and maintained indefinitely for an isolated, perfectly spherical particle. The particles' shape irregularities, surface imperfections, and interactions with the neighbors lead to a finite persistence length, which is illustrated by exemplary trajectories in (Fig. 1a).

It was demonstrated previously[17,19] that a set of dynamic collective phases can be observed in an ensemble of ferromagnetic rollers in response to activity changes. Fascinating intermittent flocks and vortex patterns have been reported in a certain narrow band of excitation frequencies. At low and high field frequencies, a gas-like state is realised in the magnetic roller system, characterised by negligible space and time velocity correlations of the rollers. We perform our experiments at $f=60$Hz, where the system of rollers is in the gas state and no collective effects are observed. Due to the nature of the particles, they may occasionally stop rolling, either because of demagnetization or temporary adhesion to the substrate. In our analysis we therefore employ filters based on the time averaged root mean square velocity (v_{rms}) per particle trajectories and particles that are not behaving as rollers for most of the time are not considered in the statistical analysis. All experimental observations are performed only in the central region of the container to avoid any edge effects. The recordings are captured by a high-speed CCD camera (Redlake MotionPro) with a sufficiently high frame rate (125 fps) to guarantee reliable particle tracking. The velocity was extracted from the distance traveled by a roller in 0.032s (4 camera frames) corresponding to about two field periods ($2/f_0$). The image and data analysis of the time sequences were performed by ImageJ, Matlab, and Mathematica. Particle tracking was done by a MATLAB script based on the Crocker and Grier algorithm[21]. We explored changes of two orders of magnitude (Fig. 1b) in the number of active particles per area (S_A) between $0.4-10.4\,\mathrm{mm}^{-2}$, which corresponds to a packing fraction ϕ in the range $0.016-0.618$. At high packing fractions, rollers start to escape in the vertical direction and occasionally leap over each other. For experiments with inert particles we used 150μm diameter glass beads to match the size of the active rollers.

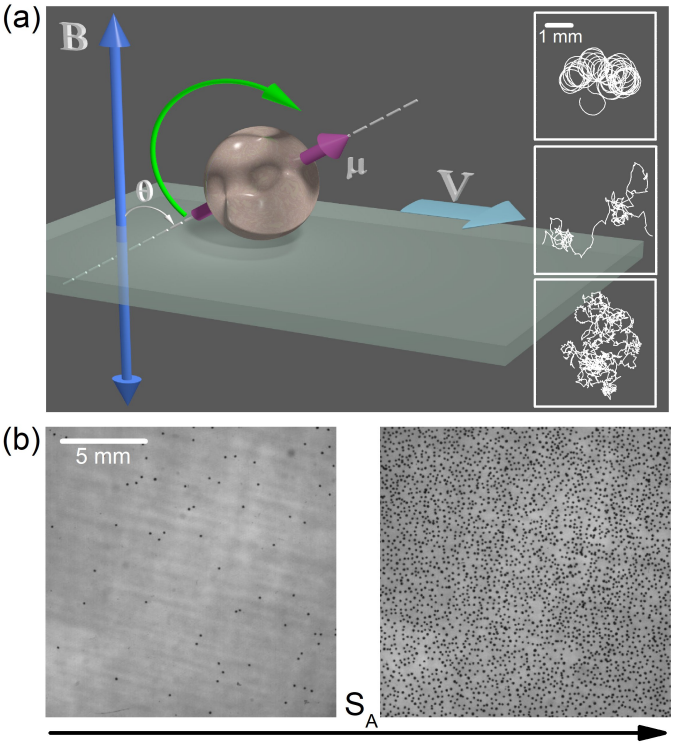

Fig. 1 Ferromagnetic rollers. (a) A sketch of the experimental system: the uniaxial vertical alternating magnetic field **B** is used to energise the ferromagnetic particles (similar as in Ref.[17]). Steady particle rotations emerging in a certain range of the excitation field parameters result in a translational motion of the particles. The right panels display three examples of roller trajectories. Characteristic persistence length l_p is about 200 μm. (b) Snapshots of the lowest $S_A=0.4\,\mathrm{mm}^{-2}$ and the highest $S_A=10.4\,\mathrm{mm}^{-2}$ experimental particle densities used in the analysis.

2.2 Model and Simulations

In addition to the experimental studies, we performed detailed numerical simulations to capture the observed dynamics and displacement statistics of active rollers and inert particles in the bath of the rollers. Magnetic particles in the simulations are modeled as spheres with radius a_i having magnetic moments μ_i. The average particle radius is given by $a=\langle a_i\rangle$ and average magnetic moment by $\mu=\langle\mu_i\rangle$. Since the particle mass density ρ_p is considered constant, the mass of particle i can be written as $m_i=ma_i^3/a^3$. Similarly for the moments of inertia as $I_i=Ia_i^5/a^5$, with $I=\frac{2}{5}ma^2$. All particles are described by their center of mass coordinate $\boldsymbol{r}_i$, angular velocity $\boldsymbol{\Omega}_i$, and (unit) direction of the magnetization $\hat{\boldsymbol{u}}_i$. As the particles roll on a flat surface, we assume that their motion is 2-dimensional, $\boldsymbol{r}_i=(x_i,y_i,0)$. The magnetic field is perpendicular to the surface and has the form $\boldsymbol{B}=B_0[0,0,\sin(\omega_0 t)]$.

We calculate the hydrodynamic drag coefficients of a particle using the result for a sphere near a no-slip boundary in the low Reynolds number regime[22]. We estimate that the distance between a particle and the surface is $d=0.01\,a$, which gives us the relative drag coefficients for translation $\psi_{TT}=6\pi\eta a\tilde{\psi}_{TT}$ with $\tilde{\psi}_{TT}=3.34$, rotation around the horizontal axis $\psi_{RR}=8\pi\eta a^3\tilde{\psi}_{RR}$ with $\tilde{\psi}_{RR}=2.25$, rotation around the vertical axis $\phi_{RR}=8\pi\eta a^3\tilde{\phi}_{RR}$ with $\phi_{RR}=1.2$ and the off-diagonal term $\psi_{TR}=8\pi\eta a^2\tilde{\psi}_{TR}$ with $\tilde{\psi}_{TR}=0.28$. $\eta\approx0.002\,$Pa s denotes the viscosity of the fluid surrounding the particles.

The equations of motion for the particles can then be written

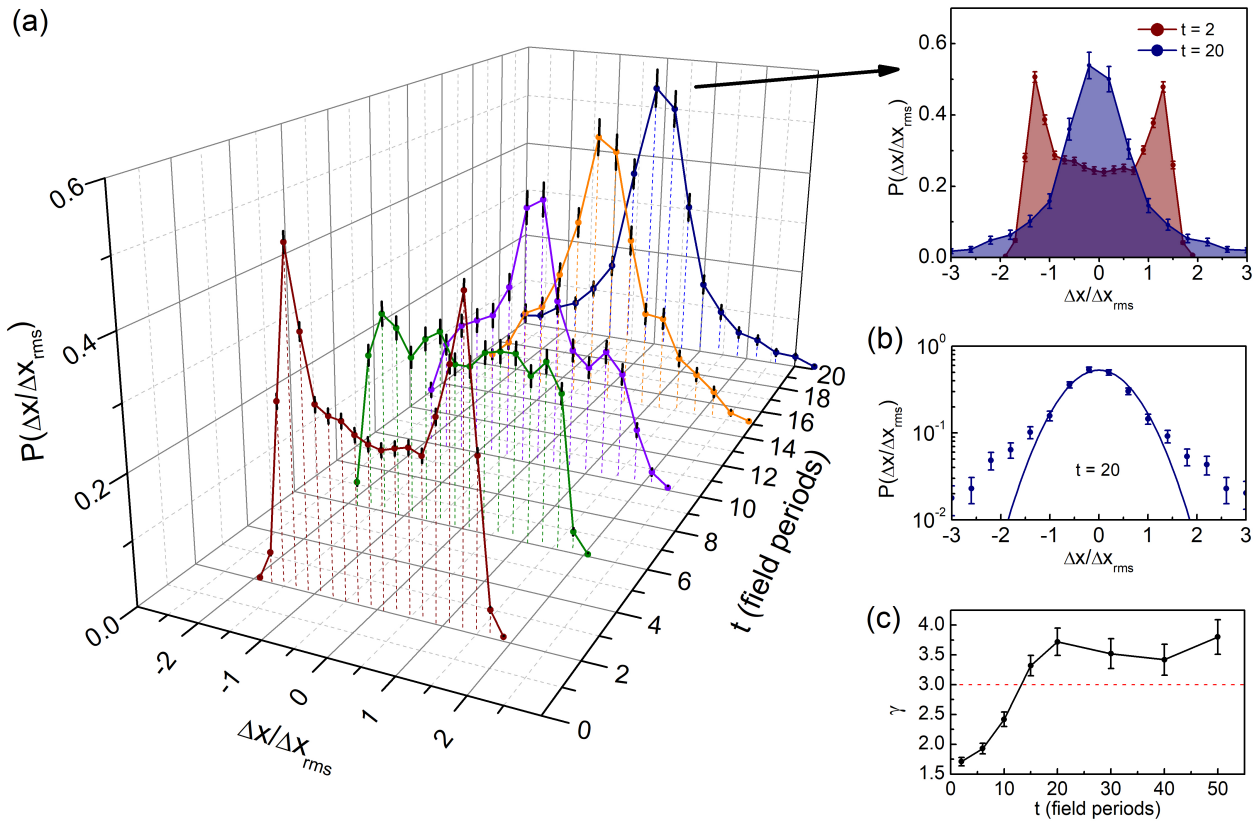

Fig. 2 Experimentally determined time evolution of area normalized probability distributions $P(\Delta x/\Delta x_{rms})$, where Δx_{rms} is the root mean square displacement. Time steps are measured in magnetic field periods ($f_B = 60\,\mathrm{Hz}$), $S_A = 0.4\,\mathrm{mm}^{-2}$. (a) The shape of $P(\Delta x/\Delta x_{rms})$ changes from multimodal (two peaks) to a distribution with Gaussian core. The plot in the top right corner shows a projection of the distributions at the time extremes ($t = 2, 20$) of the three dimensional plot. The distributions are averaged over 5000 trajectories. The area of the distributions is normalized to 1. (b) A semi-logarithmic representation of $P(\Delta x/\Delta x_{rms})$ at $t = 20$, where a Gaussian function (solid line is the best fit) describes the core well, yet the tails are overpopulated. (c) The time evolution of the Kurtosis γ showing a shift from bimodal distribution to overpopulated tails compared to a Gaussian distribution (red dashed line). The system reaches a steady distribution after sufficient time steps. Errors were estimated from repeated measurements for all panels.

as

$$m_i \frac{d\boldsymbol{v}_i}{dt} = -\psi_{TT,i}\boldsymbol{v}_i + \psi_{TR,i}\boldsymbol{\Omega}_i \times \hat{\boldsymbol{n}} + \boldsymbol{F}_i \tag{1}$$

$$I_i \frac{d\boldsymbol{\Omega}_i}{dt} = -(\psi_{RR,i}(\boldsymbol{I} - \hat{\boldsymbol{n}}\hat{\boldsymbol{n}}^T) + \phi_{RR,i}\hat{\boldsymbol{n}}\hat{\boldsymbol{n}}^T)\boldsymbol{\Omega}_i + \psi_{TR,i}\hat{\boldsymbol{n}} \times \boldsymbol{v}_i + \boldsymbol{T}_i + \mu_i \hat{\boldsymbol{u}}_i \times \boldsymbol{B} + \alpha_r \boldsymbol{\xi}_i \times \hat{\boldsymbol{u}}_i \tag{2}$$

$$\frac{d\boldsymbol{r}_i}{dt} = \boldsymbol{v}_i \tag{3}$$

$$\frac{d\hat{\boldsymbol{u}}_i}{dt} = \boldsymbol{\Omega}_i \times \hat{\boldsymbol{u}}_i\,. \tag{4}$$

$\boldsymbol{\xi}_i$ describes a Gaussian distributed noise with zero mean and variance $\langle \boldsymbol{\xi}_i(t) \otimes \boldsymbol{\xi}_i(t') \rangle = 2D_{\mathrm{R}} I_i \delta(t-t')\mathbf{I}$, where $\mathbf{I}$ is the unit tensor. The noise term reflects imperfections of the particles surface and in general largely exceeds thermal noise. $\hat{\boldsymbol{n}}$ is a unit vector normal to the surface. The expressions for force $\boldsymbol{F}_i$ and torque $\boldsymbol{T}_i$ are given by

$$\boldsymbol{F}_i = \boldsymbol{F}_i^{(\mathrm{dp})} + \boldsymbol{F}_i^{(\mathrm{hdyn})} + \boldsymbol{F}_i^{(\mathrm{hc})} \tag{5}$$

$$\boldsymbol{T}_i = \boldsymbol{T}_i^{(\mathrm{dp})} + \boldsymbol{T}_i^{(\mathrm{hdyn})} + \boldsymbol{T}_i^{(\mathrm{ani})} \tag{6}$$

where (dp) indicates forces and torques due to magnetic dipole interactions, (hdyn) due to hydrodynamics (also partially captured in the drag coefficients), (hc) indicates 'hard core' repulsive forces, and (ani) the torque resulting from anisotropic shape of particles. Magnetic dipole-dipole interactions are described through the potential

$$U_{ij}^{(\mathrm{dp})} = \frac{\mu_0 \mu_i \mu_j}{4\pi r_{ij}^3}\left[\hat{\boldsymbol{u}}_i \cdot \hat{\boldsymbol{u}}_j - \frac{3(\hat{\boldsymbol{u}}_i \cdot \boldsymbol{r}_{ij})(\hat{\boldsymbol{u}}_j \cdot \boldsymbol{r}_{ij})}{r_{ij}^2}\right], \tag{7}$$

where $r_{ij} = |\boldsymbol{r}_{ij}|$, $\boldsymbol{r}_{ij} = \boldsymbol{r}_j - \boldsymbol{r}_i$, resulting in

$$\boldsymbol{F}_i^{(\mathrm{dp})} = -\nabla_{r_i} \sum_{j \neq i} U_{ij}^{(\mathrm{dp})} \tag{8}$$

$$\boldsymbol{T}_i^{(\mathrm{dp})} = \hat{\boldsymbol{u}}_i \times \left(-\nabla_{u_i} \sum_{j \neq i} U_{ij}^{(\mathrm{dp})}\right). \tag{9}$$

For the hard core interaction, we use the WCA potential

$$U_{ij}^{(\mathrm{hc})} = \begin{cases} 4\varepsilon\left[\left(\frac{a_i+a_j}{r_{ij}}\right)^{12} - \left(\frac{a_i+a_j}{r_{ij}}\right)^{6}\right] + \varepsilon, & r_{ij} \leq 2^{1/6}(a_i+a_j) \\ 0 & r_{ij} > 2^{1/6}(a_i+a_j) \end{cases} \tag{10}$$

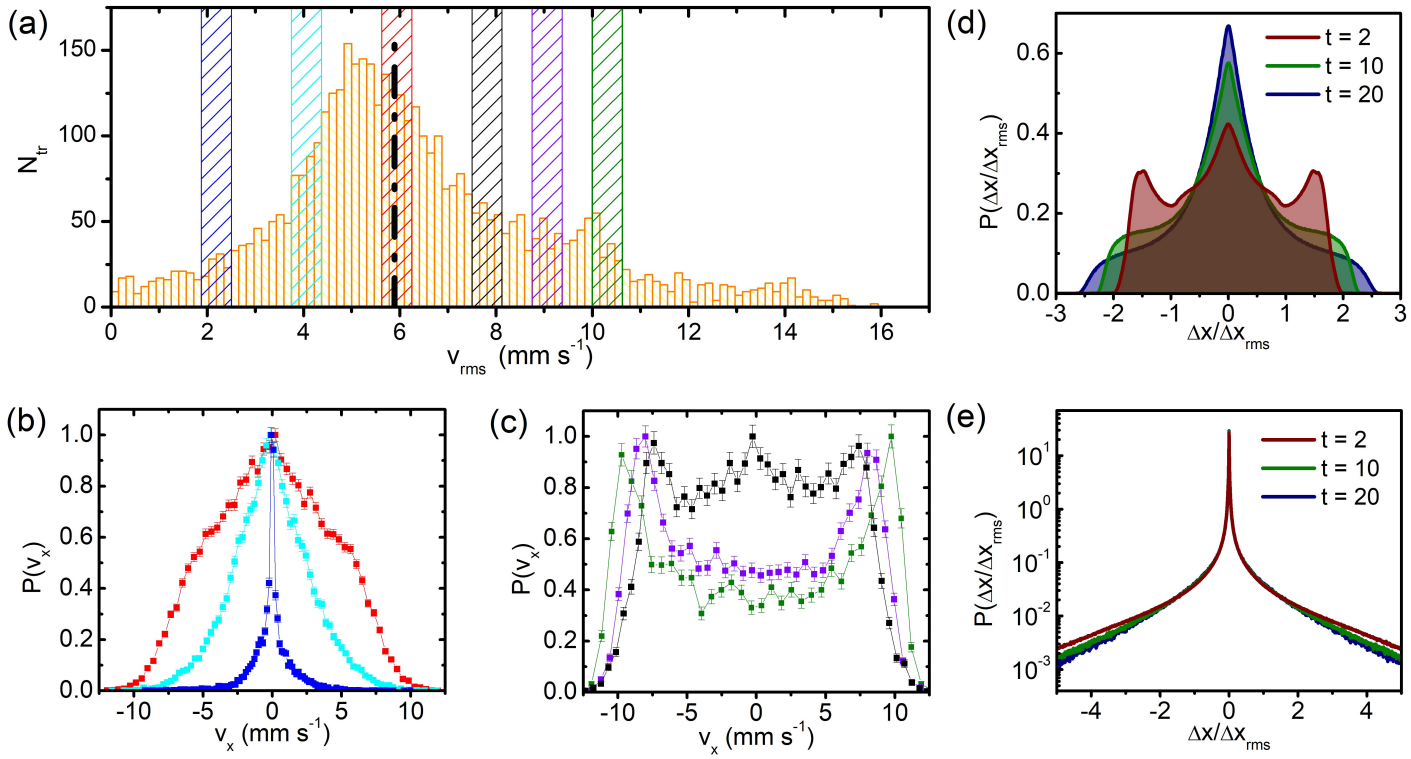

Fig. 3 (a) Histogram of the root mean square velocities v_{rms} of the rollers, time averaged over their trajectories. Each trajectory contributes only one count in the histogram. (b,c) The velocity distribution histograms $P(v_x)$ obtained from different bands of the histogram. Each $P(v_x)$ is constructed from a group of trajectories whose root mean square velocity, v_{rms}, falls within a band of the same color in the histogram. The distributions are normalized to have 1 as a maximum value.The dashed line marks the mean rolling speed of $0.2\omega R$ (similar to ref.[17]). $S_A = 0.4\,\mathrm{mm}^{-2}$. Errors were estimated from repeated measurements for panels (a)-(c).(d) Normalised displacement statistics of rollers $P(\Delta x/\Delta x_{rms})$ at different times as obtained from simulations.The area of the distributions is normalized to 1. $S_A = 3\,\mathrm{mm}^{-2}$. The data corresponds to the experimental case shown in Fig.2. (e) Statistics of inert particle displacements $P(\Delta x/\Delta x_{rms})$ as obtained from simulations. The distribution functions are dominated by a central peak at all times (note the logarithmic probability scale). $S_A = 3\,\mathrm{mm}^{-2}$ for active rollers.

with $\varepsilon = 1\times10^{-8}\,\mathrm{J}$ and the force

$$\boldsymbol{F}_i^{(\mathrm{hc})} = -\nabla_{r_i}\sum_{j\neq i} U_{ij}^{(\mathrm{hc})}\,. \tag{11}$$

While treating the particles as spherical elsewhere, we introduce an additional anisotropy term that accounts for their oblate spheroidal shape. If $\hat{\boldsymbol{f}}_i$ is a unit vector along the short axis of the ellipsoid (we assume it has a random orientation with respect to the particle's magnetization $\hat{\boldsymbol{u}}_i$), its potential is

$$U_i^{(\mathrm{ani})} = -\bar{m}_i g \varepsilon_i a_i (\hat{\boldsymbol{f}}_i\cdot\hat{\boldsymbol{n}})^2 \tag{12}$$

where g is the gravitational acceleration, $\bar{m}_i$ a particle's mass, reduced by the mass of the displaced fluid, and $\varepsilon_i = 1 - b_i/a_i$ its "eccentricity" (a_i, b_i are the long/short half-axis, respectively). $\varepsilon_i \approx 0.3$ in our experiments. The resulting restoring torque is

$$\boldsymbol{T}_i^{(\mathrm{ani})} = \hat{\boldsymbol{f}}_i \times \left(-\nabla_{f_i} U_i^{(\mathrm{ani})}\right). \tag{13}$$

This is a purely gravitational term: if a particle is not perfectly spherical, it tends to lie on its flat side in equilibrium. In that case, the potential U(ani) has a minimum and the surface normal ($\hat{\boldsymbol{n}}$) and the short axis vector ($\hat{\boldsymbol{f}}$) are aligned, which results in a zero torque on the particle. Otherwise, there is an additional torque on the particle, which wants to flip it on its flat side.

We include the hydrodynamic interactions between particles in a far-field approximation by assuming that the motion of other particles induces a shear flow with the profile $\boldsymbol{v}(z) = \boldsymbol{\Gamma} z$. The shear flow induces the following forces and torques on the particles[22]

$$\boldsymbol{F}_i^{(\mathrm{hdyn})} = \psi_{\mathrm{TD},i}\boldsymbol{\Gamma}_i \tag{14}$$

$$\boldsymbol{T}_i^{(\mathrm{hdyn})} = \psi_{\mathrm{RD},i}\hat{\boldsymbol{n}}\times\boldsymbol{\Gamma}_i \tag{15}$$

with $\psi_{\mathrm{TD},i} = 6\pi\eta a_i^2\tilde{\psi}_{\mathrm{TD}}$ ($\tilde{\psi}_{\mathrm{TD}} \approx 1.7$) and $\psi_{\mathrm{RD},i} = 8\pi\eta a_i^3\tilde{\psi}_{\mathrm{RD}}$ ($\tilde{\psi}_{\mathrm{RD}} \approx 0.47$).

A horizontal rotlet (velocity field due to a point torque) close to the surface produces a far field flow with the velocity[23]

$$\boldsymbol{v}(\boldsymbol{x}) = \frac{3}{4\pi\eta}\left[(\boldsymbol{T}\times\hat{\boldsymbol{n}})\cdot\boldsymbol{x}\right]\frac{\boldsymbol{x}\cdot\hat{\boldsymbol{n}}}{|\boldsymbol{x}|^5}\boldsymbol{x}. \tag{16}$$

For the shear rate at the surface we therefore use the ansatz

$$\boldsymbol{\Gamma}_i = 12c\sum_{j\neq i}\frac{a_j^3}{r_{ij}^5}\left[(\boldsymbol{\Omega}_j\times\hat{\boldsymbol{n}})\cdot\boldsymbol{r}_{ij}\right]\boldsymbol{r}_{ij} \tag{17}$$

with the prefactor $c \approx 0.3$.

These equations are discretized and solved in parallel on GPUs or, using OpenMP, on CPUs for different particle densities. Inert

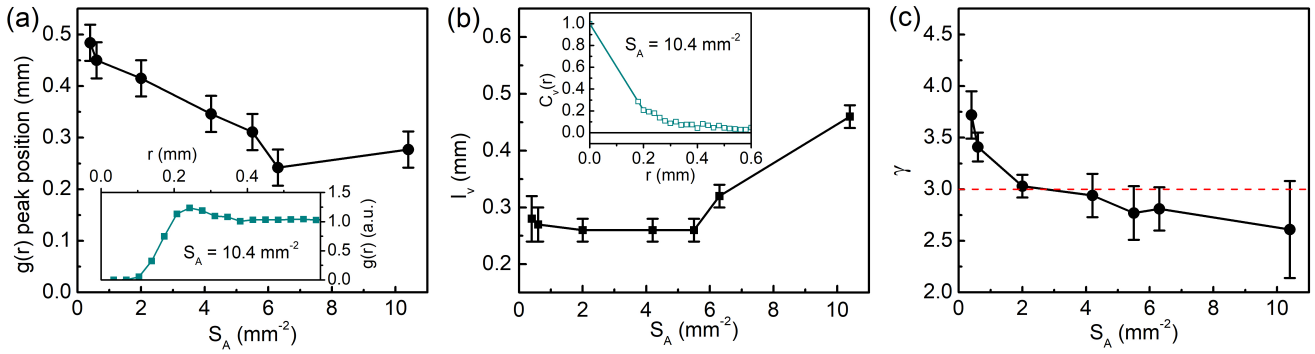

Fig. 4 Density dependence of the statistical properties of rollers. (a) Peak of the radial distribution function $g(r)$ as function of density. Insert: $g(r)$ at the largest density. The peak position steadily decreases before it plateaus at $S_A \approx 6\,\mathrm{mm}^{-2}$. (b) Velocity space correlation length l_v as function of density of active rollers S_A. Insert: The velocity space correlation function $C_v(r)$. (c) Kurtosis γ of the displacement distribution function as function of S_A. Statistics are taken at $t = 20$ field periods. Errors were estimated from repeated measurements for all panels.

particles are modeled by $\mu_i = 0$ and different mass density.

A similar approach was successfully applied previously[17] to correctly capture the emergent collective dynamics of the magnetic rollers even though the Reynolds number is $\mathrm{Re} \sim 2-4$. Naturally, to better account for the three-dimensional hydrodynamics and finite Reynolds numbers, Navier-Stokes equations need to be solved with multiple solid inclusions. A *Smoothed Particle Hydrodynamics* technique was recently employed for this task[24], which successfully captured the 3d flows induced by magnetic rollers and the resulting collective dynamics. However, this technique becomes computationally extremely expensive for large roller ensembles, which is the case in our present studies.

3 Results and Discussion

A typical time evolution of the displacement statistics of a ferromagnetic roller gas is illustrated in Fig. 2a. At short times ($t = 2$ field periods) the observed displacement distributions $P(\frac{\Delta x}{\Delta x_{\mathrm{rms}}})$ is bimodal with two distinct non-central peaks. The shape of the distribution reflects the fact of having an ensemble of particles with a constant speed v_0 and a uniformly distributed direction of travel φ. Both velocity components $(v_x, v_y) = v_0(\cos\varphi, \sin\varphi)$ are thus non-uniformly sampled in a Cartesian coordinate system and the transformed probability density function for components of the velocity yields $P(v_m) = \frac{1}{\pi v_0 \sqrt{1-(v_m/v_0)^2}}$, here $m = x, y$. The distribution is normalized to 1. The resulting displacement statistics curve has two asymptotes at $\pm v_0$ that get spread out into the distribution peaks in the presence of noise and non-uniformities in the ensemble. Wide distribution in the speeds of the active particles within the ensemble or low persistence length may completely smear the peaks, which is one of the reasons such distributions often are not reported for active systems. However, the double peak splitting was reported for Janus particles at high hydrogen peroxide (H_2O_2) concentrations, where rotational diffusion was suppressed[25]. In our system the main source of peak widening comes from the particle size distribution, shape anisotropy, and demagnetisation events that translate into a wide v_0 distribution[17].

With increasing time it becomes more likely that the particles experience collision interactions (near-field magnetic, hydrodynamic or steric), that result in a flattening of the displacements distributions $P(\Delta x/\Delta x_{\mathrm{rms}})$ (see Fig. 2a, $t = 6$) and the development of a Gaussian core (Fig. 2a at $t = 20$ and Fig. 2b). The whole distribution, however, remains non-Gaussian since the Gaussian core is accompanied by overpopulated high displacements tails, see Fig. 2b, a feature that survives for a very long time (seconds in our case) and could be also be tracked by observation of the distribution's kurtosis γ, defined as the ratio of the fourth and the squared second moments:

$$\gamma = \frac{\mu_4}{{\mu_2}^2}\,, \quad \text{here} \quad \mu_m = (1/N)\sum_{i=1}^{N}(\Delta x_i - \langle \Delta x \rangle)^m,$$

where N is the total number of events and the angle brackets represent the mean value. The kurtosis value for a Gaussian distribution is $\gamma = 3$ and is shown in Fig. 2c as a dashed red line. In a gas of ferromagnetic rollers the kurtosis of the displacement distributions at short times is significantly lower ($\gamma \sim 1.7$) and increases with time, reflecting the evolution of the distribution shape from a bimodal to a nearly Gaussian shape. However, the value of the kurtosis crosses the Gaussian value and reaches $\gamma \sim 3.7$, indicating that the distribution of displacements is still strongly non-Gaussian. Noteworthy to mention is that the non-Gaussian shape of the displacement distributions was observed for all studied roller densities and was the most pronounced for the dilute cases.

Under real experimental conditions the non-uniform distribution of particle sizes and shapes, as well as events of demagnetization lead to a distribution of the rollers' velocities and occasionally to a complete stop for some of the rollers. To discriminate "defective" rollers from the statistics we use filtering procedures based on the root mean square velocity v_{rms} time averaged over the trajectory of each roller. The typical histogram of the v_{rms} for one of the experiments is shown in Fig.3a. Taking into account the whole population of particles (including temporary rolling particles) results in a velocity statistics with a pro-

nounced central peak and missing bimodal peaks (Fig.3b). Once we filter our temporary non-rolling particles, we recover the bimodal statistics (Fig.3c). The example shown was obtained for the active particle number density $S_A = 0.4\,\mathrm{mm}^{-2}$. From the histogram we select groups of trajectories with approximately similar v_{rms} (shaded color bands in Fig. 3a) and calculate $P(v_x)$ for each group separately (Fig. 3b,c; distributions are color matched to the shaded bands in the histogram). For the lowest values of v_{rms} (dark blue band and $P(v_x)$) there is an overwhelming peak at $v_x = 0$ indicative that the trajectories in this group are mostly arrested. When we increase the value of v_{rms}, the distribution develops shoulders while still being dominated by a central peak (blue and red bands). The side peaks (shoulders) appear and become of comparable magnitude to the central one (black band) with a further increase of the v_{rms} band value. Such triple peak shapes indicate that the particles are freely rolling with velocities around that band's v_{rms}, but also get temporally arrested in parts of their trajectories. At large v_{rms} magnitudes (dark and light green bands and $P(v_x)$'s) the most probable velocity is clustered only around side peaks that match the value of v_{rms} of the chosen histogram band. For the investigation of the roller gas behaviour at all roller densities, we select a cutoff $v^* = 7.35\,\mathrm{mm\,s}^{-1}$, where the central peak disappears and include only particles/trajectories with $v_{\mathrm{rms}} \geq v^*$ in our consideration.

Our experimental observations have been successfully captured by simulations. To reproduce the behavior of the experimental system we considered ellipsoidal particles and introduced a mismatch between the particles' symmetry and magnetization axes to control effectiveness of the rolling. The mismatch angle is assigned randomly, leading to an appearance of the population of particles contributing to the central peak of the displacement statistics at short times. In particular, if the anisotropy potential (12) has a minimum, when the particle is on its flat side, it can stop rolling for some time as the resulting torque from (12) tries to keep the particle in its position. The results of the simulations are displayed in Fig. 3d. As in the experiments, the distributions are strongly non-Gaussian. The presence of temporarily non-rolling particles and rollers with a spread of rolling velocities contributed to the appearance of the central peak and the smearing of the side peaks of the distributions as observed in the experiments.

We also investigated the effect of the active roller density on the build up of velocity space correlations and the resulting displacement statistics. The roller particle density is varied from very dilute ($S_A = 0.4\,\mathrm{mm}^{-2}$, corresponding packing fraction $\phi \approx 0.024$) to a dense ensemble with $S_A \approx 10.4\,\mathrm{mm}^{-2}$ or $\phi \approx 0.6$. The effect of crowding is tracked by the radial distribution function, see Fig. 4a. To characterise the velocity space correlation we introduce a correlation length scale, l_v, determined as the length at wich the velocity correlation function, $C_v(r)$ vanishes (in fact we use a finite value of 0.05 instead of zero to be well above the noise level of the statistics). We calculate $C_v(r)$ as:

$$C_v(r) = \frac{1}{N}\sum_{t}^{N} \frac{\langle \boldsymbol{v}_i(r_0,t).\boldsymbol{v}_j(r_0+r,t)\rangle_{r_0} - \langle \boldsymbol{v}_i(r_0,t)\rangle_{r_0}\langle \boldsymbol{v}_j(r_0+r,t)\rangle_{r_0}}{\langle v_i(r_0,t)^2\rangle_{r_0} - (\langle v_i(r_0,t)\rangle_{r_0})^2}.$$

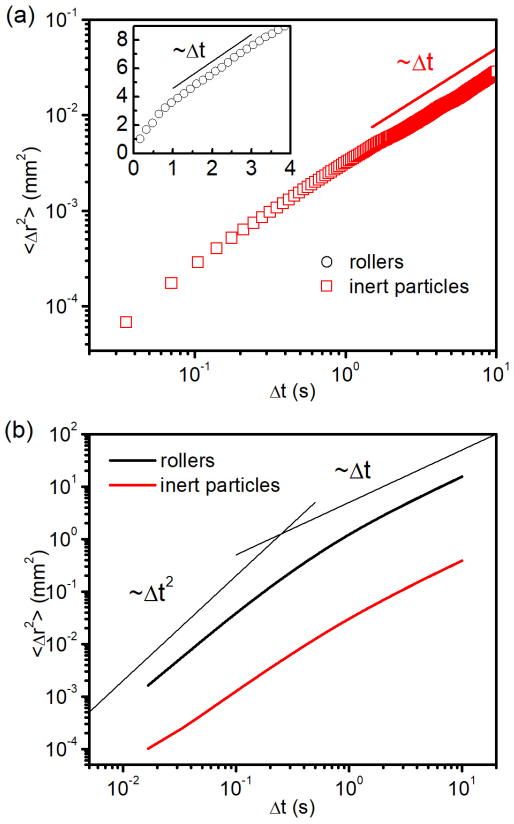

Fig. 5 (a) Mean square displacement (MSD) $\langle \Delta r \rangle^2$ versus time for inert particles (red squares) and rollers (insert). (b) MSD for active and inert particles as obtained in simulations. All curves display a clear ballistic regime at short times (black line Δt^2) and normal linear behavior at long times.

Here, $\langle \ldots \rangle_{r_0}$ denotes the average over all roller particle velocity pairs (i and j) at a particular time t, which is then averaged over the N available realizations. An example of a velocity correlation curve for $S_A \approx 10.4\,\mathrm{mm}^{-2}$ is shown in Fig. 4b. As expected, the velocity space correlation length increases with density. Previously results obtained in granular systems for velocity statistics[26] also reported accumulation of the velocity correlations with the particle density. That lead to a significant growth of the kurtosis associated with the velocity statistics (up to five times the Gaussian value). For our system at long times (diffusive regime of the system, t=20 field periods) we observe the opposite trend, see Fig. 4c, and the kurtosis of the displacement statistics gets closer to the Gaussian value with the density growth. This behavior is explained by the growth of the number of collisions experienced by a roller within a fixed time window with the density increase, making the roller displacements more and more random-like and as a result approaching Gaussian statistics.

To further quantify the diffusive properties of the active ferromagnetic roller gas we analysed the time evolution of the mean square displacement (MSD), $\langle \Delta r \rangle^2$, for both active rollers and inert particles immersed in the roller gas. Typical MSD curves for active rollers and inert particles are shown in Fig. 5a. Both curves

demonstrate normal behavior with a short ballistic region transitioning into a linear in time diffusive region. The behavior is termed normal (Fickian) and described by a $\langle \Delta r \rangle^2 = 4D_T \Delta t$ for a two-dimensional system. Here, D_T is the translational diffusion constant. Similar behavior for rollers and inert particles of the same diameter was recovered in simulations, see Fig. 5b. Thus, the active ferromagnetic roller gas displays properties of normal Brownian diffusion, while statistics of particle displacements is clearly non-Gaussian. These results could be understood within a recently proposed framework of diffusion processes with fluctuating diffusivity[15], where normal diffusive behavior arises as a result of statistical averaging over diffusivity distributions emerging due to environmental fluctuations of local diffusivity in the roller gas. In our system this distribution of local diffusivity is facilitated by the presence of long-range anisotropic interactions, namely by hydrodynamic flows generated by rotating rollers[24] and magnetic dipole-dipole interactions.

An increase in the active roller density reflects differently on the roller and inert particle diffusivities. As one can expect, the number of active particles increases the diffusivity of inert particles[18,27–30] since their motion is mostly driven by collisions with active particles. This behavior is nicely recovered in experiments with inert beads and active ferromagnetic rollers, see insert of Fig. 6. The diffusivity of the active magnetic rollers however behaves distinctively different. Upon increase of the rollers density, the average diffusivity gets suppressed. This behaviour is captured both in the experiments and simulations, Fig. 6, and can be attributed to the crowding effects of the rollers that restrict their motion. The effect becomes apparent already at relatively low rollers number densities (S_A) due to the presence of long range hydrodynamic and magnetic interactions that allow particles to "see" each other at much longer length-scales than in systems with only steric interactions. In principle, one should not expect the presented simulations to provide good quantitative agreements with the experimental data due to the fact that the model we use rely on Stokesian approximation, and all simulations results should be considered only qualitatively.

4 Conclusions

Ensembles of active ferromagnetic rollers energised by an external single-axis alternating magnetic field provide a convenient platform to investigate diffusive properties of an active magnetic roller gas with immersed inert particles. The activity in this system originates only from spinning degrees of freedom and self-propulsion emerges due to the presence of a solid interface. On the basis of experiments and simulations we demonstrate that a ferromagnetic roller gas exhibits normal Brownian diffusion with a linear in time growth of the mean-squared displacement, while statistics of displacements remains strongly non-Gaussian. The phenomenon is attributed to the strong heterogeneity of the local diffusive properties in this active system facilitated by the presence of long-range anisotropic hydrodynamic interactions and magnetic interactions. The diffusivity of inert particles embedded in the roller gas grows with the roller number density due to an increase in frequency of collisions (the only source for the motion of the inert particles) while the diffusivity of rollers gets suppressed due to crowding effects limiting the active motion of rollers. The results presented here provide new insights into diffusive properties of active systems based on spinning activity of colloids and could be used in the future design and control of transport in active systems at the microscale.

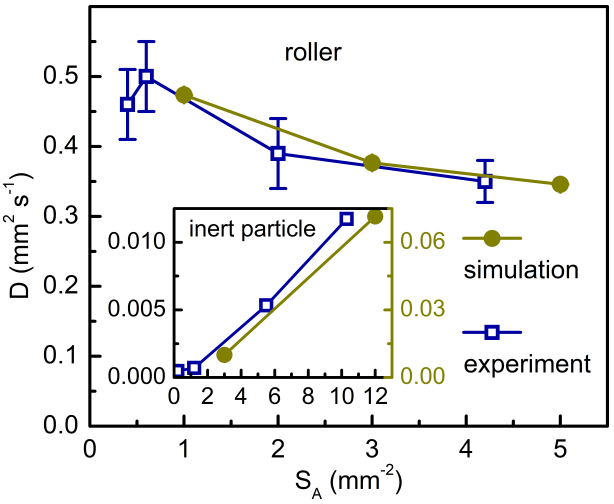

Fig. 6 Translational diffusion coefficient of active rollers and inert particles as function of the magnetic roller gas density. Errors were estimated from repeated measurements for all panels.

Acknowledgements

The research was supported by the U.S. Department of Energy, Office of Science, Basic Energy Sciences, Division of Materials Science and Engineering.

References

1 A. Zöttl and H. Stark, *Journal of Physics: Condensed Matter*, 2016, **28**, 253001.
2 I. S. Aranson, *Physics-Uspekhi*, 2013, **56**, 79.
3 A. Snezhko, *Journal of Physics: Condensed Matter*, 2011, **23**, 153101.
4 M. C. Marchetti, J.-F. Joanny, S. Ramaswamy, T. B. Liverpool, J. Prost, M. Rao and R. A. Simha, *Reviews of Modern Physics*, 2013, **85**, 1143.
5 A. Snezhko, *Current Opinion in Colloid & Interface Science*, 2016, **21**, 65–75.
6 F. Martinez-Pedrero, E. Navarro-Argemí, A. Ortiz-Ambriz, I. Pagonabarraga and P. Tierno, *Science advances*, 2018, **4**, eaap9379.
7 B. Wang, S. M. Anthony, S. C. Bae and S. Granick, *Proceedings of the National Academy of Sciences*, 2009, **106**, 15160–15164.
8 X. Zheng, B. ten Hagen, A. Kaiser, M. Wu, H. Cui, Z. Silber-Li and H. Löwen, *Physical Review E*, 2013, **88**, 032304.
9 J. Guan, B. Wang and S. Granick, *ACS nano*, 2014, **8**, 3331–3336.
10 H. Kurtuldu, J. S. Guasto, K. A. Johnson and J. P. Gollub, *Proceedings of the National Academy of Sciences*, 2011, **108**, 10391–10395.
11 K. Kohlstedt, A. Snezhko, M. Sapozhnikov, I. Aranson, J. Olaf-

sen and E. Ben-Naim, *Physical review letters*, 2005, **95**, 068001.
12 J. Van Zon and F. MacKintosh, *Physical review letters*, 2004, **93**, 038001.
13 W. Losert, D. Cooper, J. Delour, A. Kudrolli and J. Gollub, *Chaos: An Interdisciplinary Journal of Nonlinear Science*, 1999, **9**, 682–690.
14 S. Hapca, J. W. Crawford and I. M. Young, *Journal of The Royal Society Interface*, 2008, **6**, 111–122.
15 A. V. Chechkin, F. Seno, R. Metzler and I. M. Sokolov, *Physical Review X*, 2017, **7**, 021002.
16 A. Bricard, J.-B. Caussin, N. Desreumaux, O. Dauchot and D. Bartolo, *Nature*, 2013, **503**, 95.
17 A. Kaiser, A. Snezhko and I. S. Aranson, *Science Advances*, 2017, **3**, e1601469.
18 G. Kokot, S. Das, R. G. Winkler, G. Gompper, I. S. Aranson and A. Snezhko, *Proceedings of the National Academy of Sciences*, 2017, **114**, 12870–12875.
19 G. Kokot and A. Snezhko, *Nature communications*, 2018, **9**, 2344.
20 G. Kokot, D. Piet, G. M. Whitesides, I. S. Aranson and A. Snezhko, *Scientific reports*, 2015, **5**, 9528.
21 J. C. Crocker and D. G. Grier, *Journal of colloid and interface science*, 1996, **179**, 298–310.
22 B. Cichocki and R. Jones, *Physica A: Statistical Mechanics and its Applications*, 1998, **258**, 273–302.
23 J. Blake and A. Chwang, *Journal of Engineering Mathematics*, 1974, **8**, 23–29.
24 Y. Wang, S. Canic, G. Kokot, A. Snezhko and I. Aranson, *Physical Review Fluids*, 2019, **4**, 013701.
25 X. Zheng, B. ten Hagen, A. Kaiser, M. Wu, H. Cui, Z. Silber-Li and H. Löwen, *Physical Review E*, 2013, **88**, 032304.
26 D. L. Blair and A. Kudrolli, *Physical Review E*, 2001, **64**, 050301.
27 X.-L. Wu and A. Libchaber, *Physical review letters*, 2000, **84**, 3017.
28 K. C. Leptos, J. S. Guasto, J. P. Gollub, A. I. Pesci and R. E. Goldstein, *Physical Review Letters*, 2009, **103**, 198103.
29 A. Sokolov, R. E. Goldstein, F. I. Feldchtein and I. S. Aranson, *Physical Review E*, 2009, **80**, 031903.
30 A. E. Patteson, A. Gopinath, P. K. Purohit and P. E. Arratia, *Soft matter*, 2016, **12**, 2365–2372.

Diffusive properties of an active magnetic roller gas are investigated in experiments and by means of discrete particles simulations.